

Functional Nanoparticle-Augmented Surfactant Fluid for Enhanced Oil Recovery in Williston Basin

Quarterly Status Report

(for the period of November 1, 2017 through February 1, 2018)

Prepared for:

Karlene Fine
Brent Brannan

North Dakota Industrial Commission
State Capitol, 14th Floor
600 East Boulevard Avenue, Department 405
Bismarck, ND 58505-0840

Contract No.: G-041-081

Prepared by:

Hui Pu
Julia Zhao
Department of Petroleum Engineering
Department of Chemistry
University of North Dakota

Research Team Members:

Xun Zhong
Yanxia Zhou
Runxuan Sun
Xiao Liu
Wen Sun
Xu Wu

January 31, 2018

Summary of Current Progress

During the past quarter, our primary goals were to select the interested area to acquire core samples and characterized the core samples with the scanning electron microscope (SEM). Meanwhile, we tested the stability of silica nanoparticles. Furthermore, we are trying to develop polymer nanoparticles and measure their physicochemical properties.

We mainly focused on the following tasks:

- 1) Selected areas for core samples and their SEM measurement;
- 2) Pore space characterization;
- 3) Stability experiment of silica nanoparticle
 - a.) Salinity effect;
 - b.) Concentration of silica nanoparticles (wt%)
 - c.) Composition of synthetic brine water
 - d.) Lower concentrations of silica nanoparticles (wt%)
 - e.) Brines with different cation valence
- 4) Evaluation and optimization of the nanoparticle-surfactant for EOR
 - a.) Description of newly purchased nanoparticles;
 - b.) Stability test;
 - c.) Effects of pH and zeta potential test;
 - d.) Emulsion test.
- 5) Preparation and characterization of silica nanoparticles for oil recovery;
- 6) Preparation and characterization of polymer nanoparticles for oil recovery;

Below are the detailed results on the tasks.

1. Selected Areas for Core Samples and SEM Measurement

1.1 Selected areas for core samples

As shown in the map below (Figure 1), the purple line represents the boundary of high production area is outlined by the, the orange line delineates the area of high oil/(oil+water) ratio, and the black line defines an area of high pressure gradient. Middle Bakken core samples were drilled from three wells as shown in Figure 1.

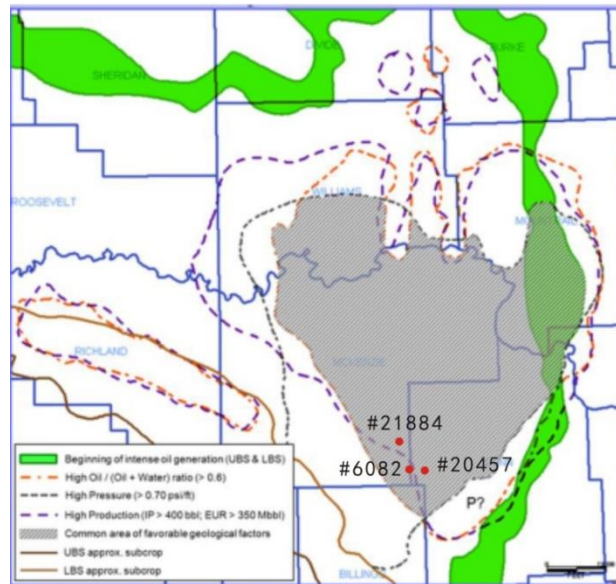


Figure 1. Selected Areas for Bakken Core Samples (Theloy and Sonnenberg, 2013)

1.2 SEM Experiment Test

1.2.1 Selection of rock samples

The first step was to determine the depth of Middle Bakken, and then chose the appropriate core samples from that depth range, according to the depth, length, development of slips, anisotropy and so on. For instance, the thickness of Bakken Formation in well #20457 is 128 ft. According to lithology, the well core can be divided into three members: Upper Bakken (Figure 2), Middle Bakken (Figure 3) and Lower Bakken (Figure 4).



Figure 2. Upper Bakken



Figure 3. Middle Bakken



Figure 4. Lower Bakken

The depth range of each member is 11,155-11,166 ft, 11,166-11,197 ft and 11,197-11,205 ft, respectively. So the Middle Bakken which is need to be analyzed is from depth of 11,166 to 11,197 ft. According to the factors mentioned above, the core samples are at 11176.6 (Figure 5), 11185.6 (Figure 6) and 11192.5 (Figure 7) ft depth.

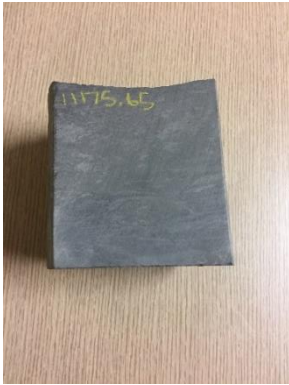


Figure 5. Core sample 1



Figure 6. Core sample 2



Figure 7. Core sample 3

For well #6082, the Upper Bakken Formation is from 10,954 to 10,968 ft and is black limestone (Figure 8). Rock from 10,968 to 10,979 ft is black shale (Figure 9). The Middle Bakken Formation ranges from 10,979 to 11,009 ft and is grey limestone (Figure 10).



Figure 8. Upper Bakken



Figure 9. Upper Bakken



Figure 10. Middle Bakken

According to the depth of formation, we obtained the rock samples at the depth of 10,957 (Figure 11), 10,983 (Figure 12) and 10,994 ft (Figure 13).



Figure 11. Rock sample 1

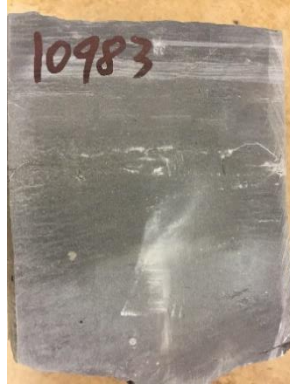


Figure 12. Rock sample 2



Figure 13. Rock sample 3

1.2.2 Core plugs

Core plugs were cored from rock samples using a drill press and coring drilling bit. The core plugs from well #20457 are showing below (Figures 14, 15, 16).



Figure 14. Core plug 1



Figure 15. Core plug 2



Figure 16. Core plug 3

During the coring process of core plug 3, the core plug broke into three small pieces. We also have got three core plugs from rock samples of well #6082 (Figures 17, 18, 19).



Figure 17. Core plug 1



Figure 18. Core plug 2



Figure 19. Core plug 3

1.2.3 SEM Analysis

Scanning electron microscopy (SEM) produces a two-dimensional (2-D) raster image by bombarding the surface of a sample with a beam of electrons and then detecting the various signals produced by the interaction between sample and electron beam (Goldstein, 2003; Reimer, 1998). SEM examines both topographic characteristics and atomic composition. This analytical technique is capable of producing very high-resolution images showing nanometer-scale features, grain size, and treatment effects. Figure 20 shows an image with a magnification of 100,000, a pore is observed with a dimension of 1,477 nm by 400 nm. Calcite crystals and quartz are showing in Figure 21.

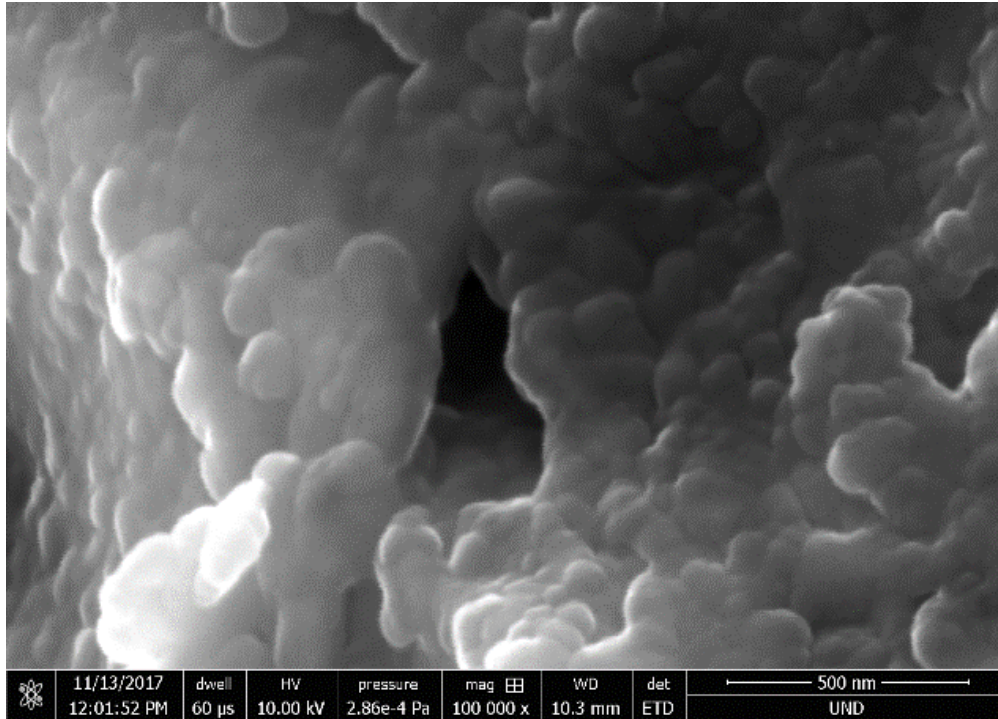


Figure 20. SEM Image of Middle Bakken displaying pore

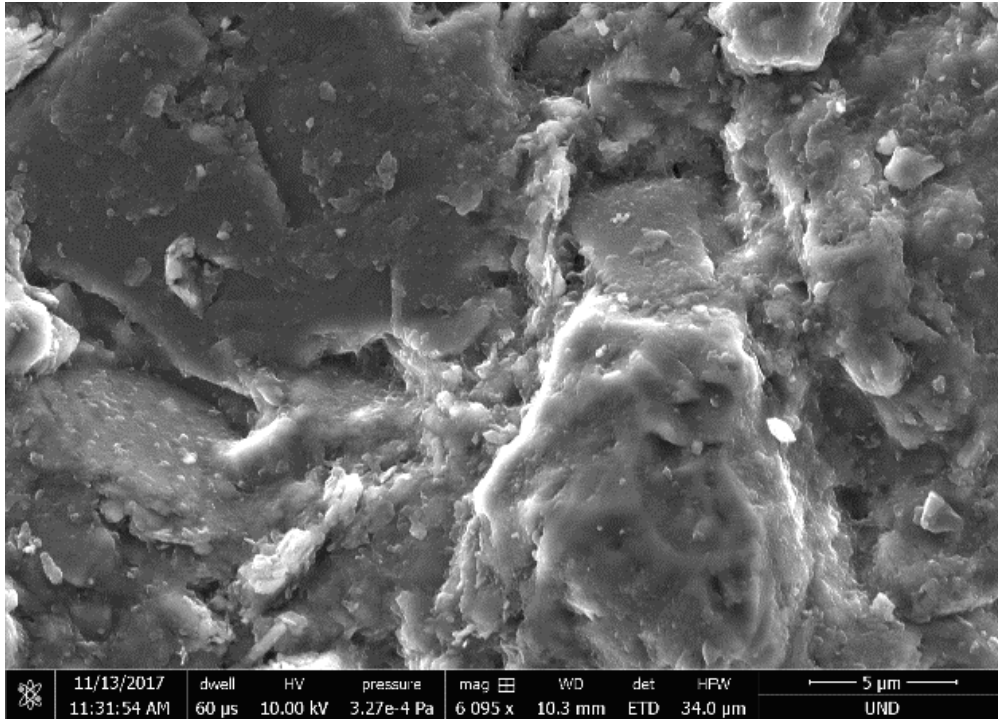
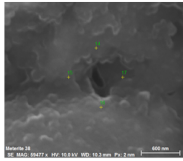


Figure 21. SEM Image of Middle Bakken

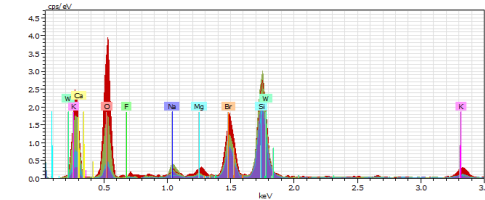
1.2.4 Automated rock characterization with SEM/image-analysis techniques

A BSE image from the SEM is digitized and stored in the IPS memory. The stored image has a standard format of 512*512 points (pixels or picture elements) in which each point can have a gray value from 0 to 255. A zero value corresponds to black (pores) and ranges from gray (quartz) to white (heavy minerals), which is 255.

The pores are determined from the mineral components in the image by detecting only the dark areas. Mathematical morphology techniques allow individual pores to be defined. Pore area and pore-throat-size distributions are measured, as is the 2D coordination number. The results are shown in Figure 22.



Meterite 38Date:11/14/2017 11:40:09 AMImage size:1200 x 1036Mag:59477.4176169525xHV:10.0kV



14 Date:11/14/2017 11:40:50 AM HV:10.0kV Puls th:0.65kcps
 15 Date:11/14/2017 11:41:00 AM HV:10.0kV Puls th:0.98kcps
 16 Date:11/14/2017 11:41:11 AM HV:10.0kV Puls th:1.24kcps
 17 Date:11/14/2017 11:41:21 AM HV:10.0kV Puls th:0.63kcps

Norm. mass percent (%)

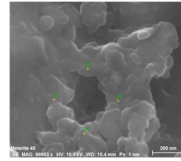
Spectrum	O	F	Na	Mg	Si	K	Ca	Br	W
14	24.05	- 0.76	- 40.50	3.77	- 24.83	16.09	-	-	-
15	28.52	- 2.92	- 35.58	2.46	- 19.80	10.51	-	-	-
16	39.32	0.86	0.86	1.12	21.69	5.37	2.23	19.85	0.86
17	10.22	- 1.54	- 44.00	2.03	2.41	24.04	15.75	-	-

Mean value: 23.03 0.86 1.54 1.12 35.44 3.46 2.32 22.06 12.80
 Sigma: 13.42 0.00 0.97 0.00 9.80 1.47 0.13 2.76 3.66
 Sigma mean: 6.71 0.00 0.49 0.00 4.90 0.73 0.06 1.38 1.83

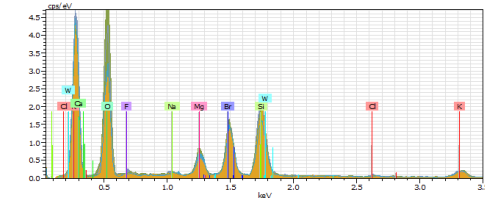
11/14/2017

1. Page

(Quartz)



Meterite 40Date:11/14/2017 12:12:25 PMImage size:1200 x 1036Mag:99903.4749034749xHV:10.0kV



22 Date:11/14/2017 12:12:59 PM HV:10.0kV Puls th:1.24kcps
 23 Date:11/14/2017 12:13:09 PM HV:10.0kV Puls th:1.47kcps
 24 Date:11/14/2017 12:13:20 PM HV:10.0kV Puls th:1.41kcps
 25 Date:11/14/2017 12:13:30 PM HV:10.0kV Puls th:1.23kcps

Norm. mass percent (%)

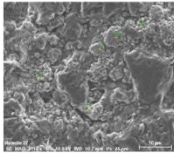
Spectrum	O	F	Na	Mg	Si	Cl	K	Ca	Br	W
22	42.57	1.60	- 4.28	18.22	- 4.09	9.90	19.35	-	-	-
23	52.00	-	- 3.86	17.54	- 3.68	6.49	14.47	-	-	-
24	46.66	2.21	0.51	2.69	20.38	0.67	5.02	4.52	17.36	-
25	39.37	1.63	- 2.89	18.61	- 4.60	6.22	19.01	7.66	-	-

Mean value: 45.15 1.82 0.51 3.43 18.69 0.67 4.34 6.78 18.04 7.66
 Sigma: 5.46 0.34 0.00 0.76 1.21 0.00 0.60 2.25 1.36 0.00
 Sigma mean: 2.73 0.17 0.00 0.38 0.60 0.00 0.30 1.13 0.68 0.00

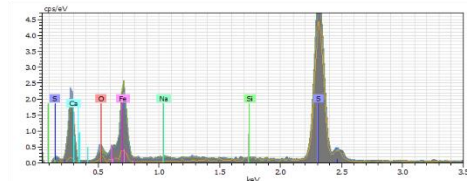
11/14/2017

1. Page

(Dolomite)



Meterite 37Date:11/14/2017 11:05:50 AMImage size:1200 x 1036Mag:3117.88086346709xHV:10.0kV



9 Date:11/14/2017 11:12:28 AM HV:10.0kV Puls th:1.59kcps
 10 Date:11/14/2017 11:12:39 AM HV:10.0kV Puls th:1.54kcps
 11 Date:11/14/2017 11:12:49 AM HV:10.0kV Puls th:1.00kcps
 12 Date:11/14/2017 11:12:59 AM HV:10.0kV Puls th:1.47kcps
 13 Date:11/14/2017 11:13:10 AM HV:10.0kV Puls th:1.57kcps

Norm. mass percent (%)

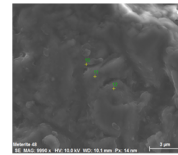
Spectrum	O	Na	Si	S	Ca	Fe
9	3.96	-	- 42.80	- 53.23	-	-
10	6.42	0.59	- 49.81	- 44.10	-	-
11	1.57	- 0.59	45.84	1.91	50.10	-
12	3.23	-	- 52.47	- 44.10	-	-
13	3.00	-	- 51.85	- 45.15	-	-

Mean value: 3.63 0.59 0.59 48.40 1.91 47.35
 Sigma: 1.78 0.00 0.00 4.13 0.00 4.11
 Sigma mean: 0.80 0.00 0.00 1.85 0.00 1.84

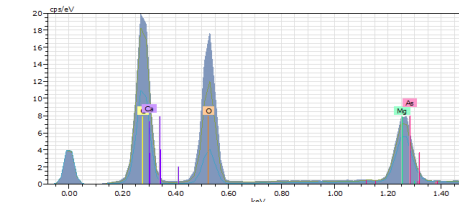
11/14/2017

1. Page

(Pyrite)



Meterite 48Date:11/16/2017 12:06:49 PMImage size:1200 x 1036Mag:9009.24740934749xHV:10.0kV



10 Date:11/16/2017 12:07:26 PM HV:10.0kV Puls th:2.56kcps
 11 Date:11/16/2017 12:07:47 PM HV:10.0kV Puls th:3.69kcps
 12 Date:11/16/2017 12:08:08 PM HV:10.0kV Puls th:4.29kcps

Norm. mass percent (%)

Spectrum	C	O	Mg	Ca	As
10	42.20	22.67	9.75	21.34	4.04
11	41.68	35.63	6.91	13.24	2.54
12	38.32	41.27	6.58	11.08	2.75

Mean value: 40.79 33.19 7.75 15.22 3.11
 Sigma: 2.11 9.54 1.74 5.41 0.81
 Sigma mean: 1.22 5.51 1.01 3.12 0.47

11/16/2017

1. Page

(Dololimestone)

Figure 22. Automated Rock Characterization of different minerals

2. Pore space characterization

Since the Bakken formation is too tight to be described using conventional methods, the Scanning electron microscope (SEM) was utilized to identify the pores and look down into the pores to characterize pore connection in rocks. Gas adsorption technique was also used to characterize pore surface area and volume in mudrocks. N₂ (at 77 K) was used in the gas adsorption experiment for surface area and mesopore characterization.

2.1. Materials and instruments

SEM materials: epoxy resin, epoxy hardener, release agent, rock sample. Figure 23 shows the prepared rock samples used in this SEM measurement.



Figure 23. Samples for SEM imaging

SEM instruments: Struers Labopol-21 grinding/polishing machine, Quanta FEG 650 scanning electron microscope.

Gas adsorption Materials: the crushed rock samples in powder was used in adsorption tests (Figure 24). Gas adsorption instrument was Autosorb iQ-Chemisorption & Physisorption Gas Sorption Analyzer.



Figure 24. Rock powder for gas adsorption

2.2 Shape features of pores and slits from SEM

In the early stages of work, we observed some inorganic pores in SEM images. More SEM images were captured using the Quanta™ FEG-650 field emission machine. An organic matter was found in the core sample (Figure 25). However, the amount of organic matter pore is so small and the dominant pore types in Middle Bakken are inorganic interparticle and intraparticle pores.

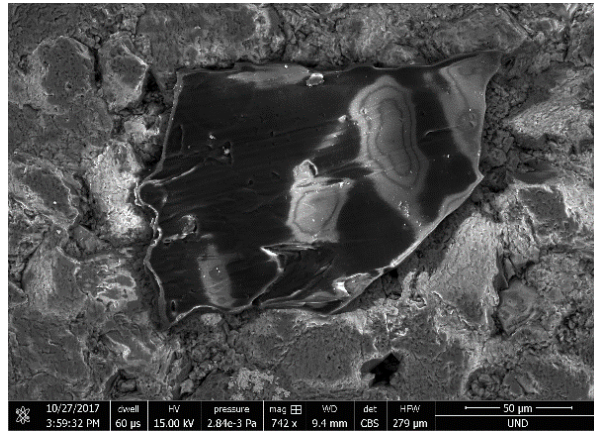


Figure 25. Organic matter in Middle Bakken

The pore networks are extremely sophisticated. As shown in Figure 26, the crack is connected with several pores, and the shapes vary greatly, also the sizes of the throats are quite small (tens of nanometers).

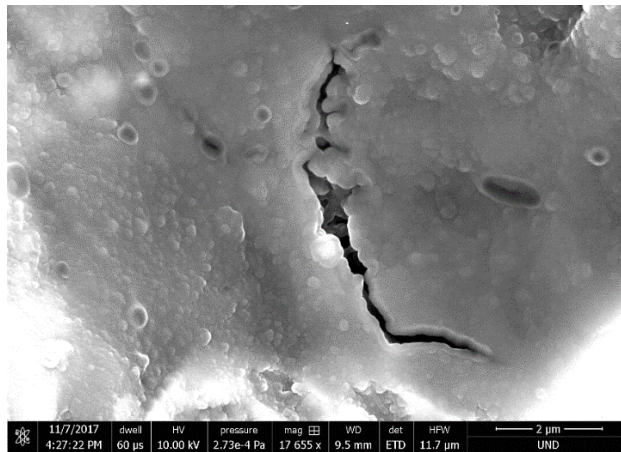


Figure 26. Natural crack in Middle Bakken

2.3 Nitrogen adsorption

Table 1 shows the 3 core samples with different permeabilities used in the nitrogen adsorption experiment to measure the adsorption isotherm. The N₂ isotherms are shown in Figure 27.

Table 1. Basic information of samples for nitrogen adsorption experiment

MD, ft	Sample	K, mD	Φ, %
11,079.50	S2	0.013	6.5
11,081.50	S3	<0.0001	7.7
11,082.50	S4	0.657	8

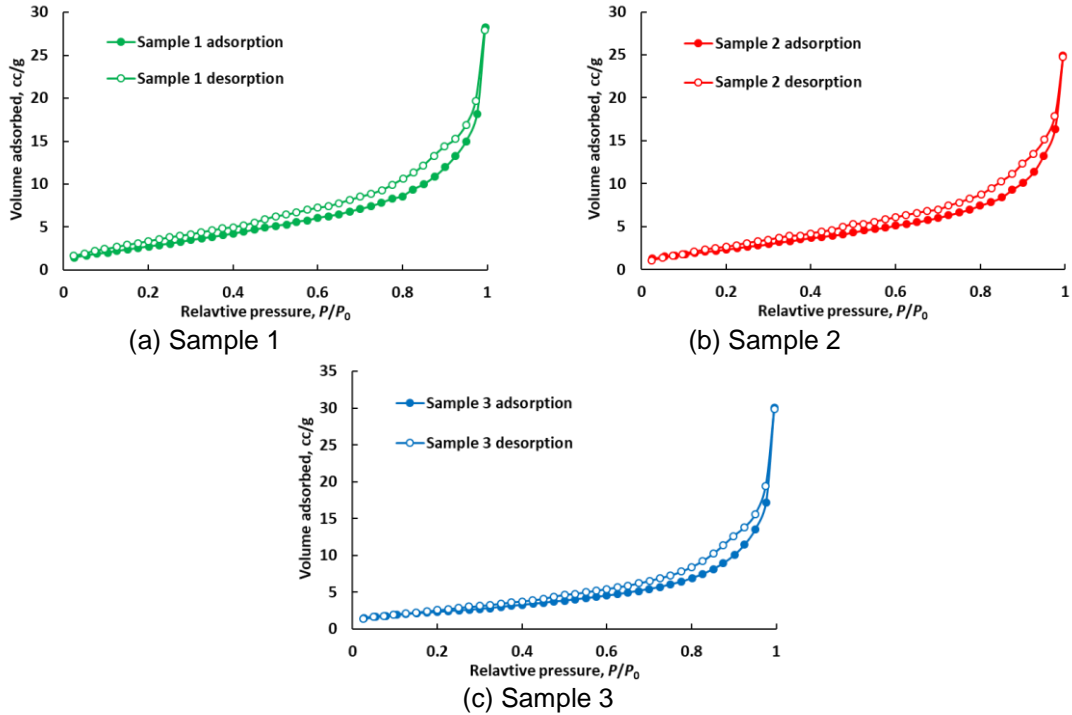


Figure 27. N₂ isotherms for the Middle Bakken samples

Since physisorption is a complex process involving various interactions, the majority of these isotherms may conveniently be grouped into six classes in the IUPAC (International Union of Pure and Applied Chemistry) classification (Figure 31, Sing et al. 1985).

- I: Microporous materials;
- II: Nonporous materials;
- III: Nonporous materials and materials which have the weak interaction between the adsorbate and adsorbent;
- IV: Mesoporous materials;
- V: Porous materials and materials that have the weak interaction between the adsorbate and adsorbent;
- VI: Homogeneous surface materials.

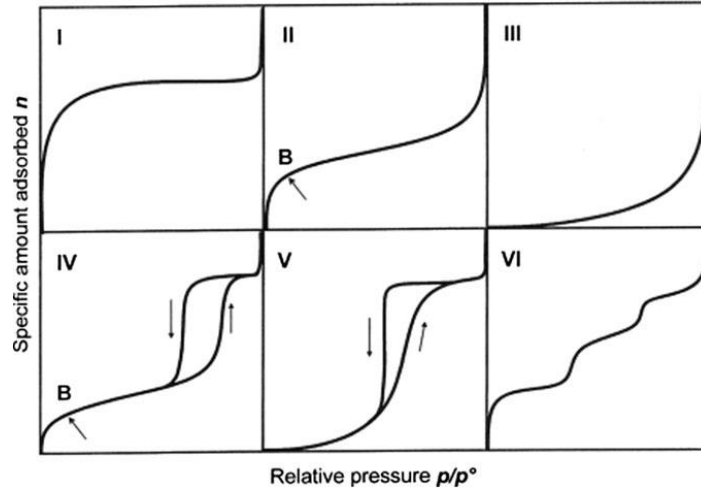


Figure 28. The six main types of gas physisorption isotherms, according to the IUPAC classification (Sing et al. 1985)

The shape of the isotherms is between III and V, which indicates an extremely small pore size and a weak interaction between the adsorbate and adsorbent.

BET method was used to quantify surface area (Brunauer et al. 1938). The surface areas of these samples were measured to be $11.185\text{m}^2/\text{g}$, $9.544\text{m}^2/\text{g}$, $8.510\text{m}^2/\text{g}$, respectively. The pore diameter distribution is shown in Figure 29. There is no significant difference between the results of 3 samples, so the difference of permeability is most likely caused by the tortuosity, as we know the pore networks in tight oil is sophisticated.

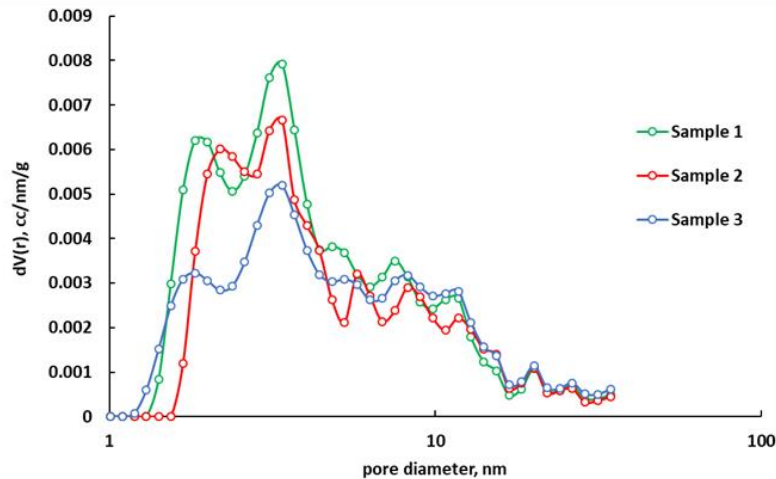


Figure 29. Pore diameter distribution

The pore diameter distribution is 2~40nm, while the dominant pore diameter is about 4 nm (Figure 29), which is extremely small. The fluid properties in such tight formation should be analyzed in the future work.

3. Stability experiment of silica nanoparticle

The experiment is to test whether the factors, such as salinity, silica nanoparticles concentration, composition of synthetic brines, and different cations, would affect the stability of silica nanoparticles. All the silica nanoparticle samples were made from high concentration silica nanoparticle solution.

3.1 Materials

Synthetic brines

There are three types of synthetic brines, i.e. NaCl solution, CaCl₂ solution and Bakken formation water. Compositional analysis of Bakken formation brine is shown in Table 2 (Lu et al. 2014). The brine in Bakken formation is highly saline with a total dissolved solid of 324,949.4mg/L.

Table 2. Compositions of Bakken formation brine

Ions	Na ⁺	K ⁺	Ca ²⁺	Mg ²⁺	Sr ²⁺	Ba ²⁺	Cl ⁻	SO ₄ ²⁻	HCO ₃ ⁻	TDS
Concentration, mg/L	101,263	6,525	17,157	1,223	1,168	30.4	196,874	409	300	324,949.4

Silica Nanoparticle

The silica nanoparticles were prepared by Stober method. The average size was about 154.1 ± 1.9 nm; and the average zeta potential was about -45.8 ± 3.9 mV. The silica nanoparticles were provided in high concentration at 160 mg/L. It was diluted to 100mg/L with ultrasonic dispersion before experiment, and then was used to prepare the silica nanoparticle solutions with different mass concentrations.

3.2 Results

3.2.1 Salinity effect

Experimental temperature was set at 80°C and experimental pressure was 1 atm. The concentration of silica nanoparticle was 0.05wt%. We prepared seven kinds of water solutions, i.e. distilled water, daily drinking water, NaCl solutions with concentrations of 30,000 mg/L, 60,000 mg/L, 120,000 mg/L, 240,000 mg/L, 300,000 mg/L, as shown in Table 3. The sample volume is 10 ml. This is to primarily test the stability of silica nanoparticle in different salinities of brines with monovalent ions.

Table 3. Seven kinds of water solution

	Distilled Water	Tap water	NaCl Solutions				
Salinity (mg/L)	0	574	30,000	60,000	120,000	240,000	300,000

Initially all the seven nanoparticle solutions were cloudy. The ultrasonic dispersion process was continued for 15 minutes to assure that nanoparticles had been homogeneously dispersed. After four days, the solution color changed (Figure 33). In the Figure 30, the samples from left to right the salinity is distilled water, tap water, and NaCl solutions with concentrations of 30,000mg/L, 60,000mg/L, 120,000mg/L, 240,000mg/L, 300,000mg/L, respectively.



a. Initial
Figure 30. Silica nanoparticle solutions in seven kinds of water solutions at initial preparation and Day 4 at 80°C

We can see from the Figure 30a that the color of left three bottles, i.e. the salinity with distilled water, tap water and 30,000mg/L, were cloudier than the rest of four bottles, namely, the salinity with 60,000mg/L, 120,000mg/L, 240,000mg/L, 300,000mg/L, respectively. After 4 days, all the bottles changed into transparent. Whether there is any aggregation at the bottom of these bottles, the size of the silica nanoparticle should be tested. Then some solutions were chosen to be tested for particle size. Every sample was tested three times. The results are shown in Table 4.

Table 4. Particle size of silica nanoparticle in different salinity brines

Times	Particle Size (nm)						
	Distilled Water	Tap water	NaCl Solutions				
			30,000	60,000	120,000	240,000	300,000
First test	--	67.87	--	--	38.04	0.00	302.0
Second test	--	26.8	--	--	141.7	268.5	911.6
Third test	--	68.9	--	--	124.4	172.3	683.6

Notes: "--" stands for the silica nanoparticle size was not tested.

We can see from the Table 4 that the size of silica nanoparticle with the salinity of 300,000mg/L is much larger than its original size 154.1 ± 1.9 nm. The size with the salinity of 240,000mg/L is a little larger, which indicates the silica nanoparticles have aggregation tendency. The other tested size is all around its original size. So the silica nanoparticle is unstable with the salinity of NaCl above 240,000mg/L.

3.2.2 Concentration of silica nanoparticles (wt%)

Experimental temperature was set at 80°C. The synthetic brine was NaCl solution, and its salinity was 30,000mg/L. We prepared five kinds of silica nanoparticle solutions, i.e. 0.1wt%, 0.2wt%, 0.3wt%, 0.4wt% and 0.5wt%. The sample volume is 10ml. This goal was to test the stability of different concentrations of silica nanoparticle in synthetic brines.



a. Initial
Figure 31. Silica nanoparticle in five different concentrations of NaCl solutions at initial preparation and Day 4 at 80°C

Initially all five silica nanoparticle solutions were cloudy. The ultrasonic dispersion process was

continued for 15 minutes to assure that nanoparticles had been homogenously dispersed. After four days, the solution changed. In the Figure 31, the samples from left to right had the concentrations of 0.1wt%, 0.2wt%, 0.3wt%, 0.4wt% and 0.5wt%. The white aggregation at bottom of 0.5wt% silica nanoparticle solution is shown in Figure 32.



Figure 32. Aggregation of silica nanoparticles solution of 0.5wt% concentration at Day 4 at 80°C

White sediment is observed at the bottom of all samples after four days. The higher the nanoparticle concentration, the more the white sediments. While there were no apparent sediments in the sample with 0.1wt% silica nanoparticle solution after four days. Its nanoparticle size could be tested to determine whether there was any aggregation in it. The sample was tested three times. The results were shown in Table 5.

Table 5. Particle size of silica nanoparticle of 0.1wt% concentration

Concentration	Particle Size (nm)		
	First test	Second test	Third test
0.1%	820.1	1024	1164

We can see from the Table 5 that the size of silica nanoparticle with the concentration of 0.1wt% is much larger than its original size 154.1 ± 1.9 nm. This indicated the silica nanoparticle had aggregated. So the silica nanoparticle is unstable with the concentration higher than 0.1wt% at 80°C.

3.2.3 Composition of synthetic brines

Experiment temperature was set at 80°C and experimental pressure was 1 atm. The concentration of silica nanoparticles was 0.05wt%. We prepared three kinds of brines, including NaCl solution (its salinity is 30,000mg/L), CaCl₂ solution (salinity: 30,000mg/L) and synthetic Bakken formation water (salinity: 324,949.4mg/L, as shown in Table 2). The sample volume is 10 ml. The goal was to test the stability of silica nanoparticles in synthetic brines of different compositions.

Initially all the solutions were cloudy. The ultrasonic dispersion process was continued for 15 minutes to assure that nanoparticles had been homogenously dispersed. After four days, the solution color changed, as shown in Figure 33. In the Figure 33, the sample from left to right were the synthetic brine solutions of NaCl solution, CaCl₂ solution and synthetic Bakken formation water, respectively.

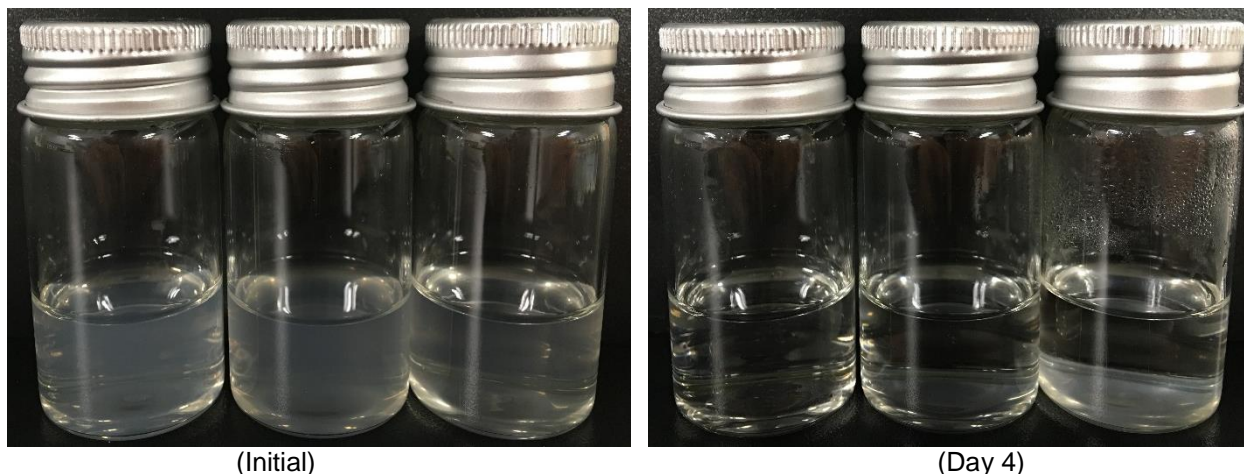


Figure 33. 0.05wt% silica nanoparticle solution in three kinds of synthetic brines at initial preparation and Day 4 at 80°C

We can see from the Figure 33 that after four days, all three silica nanoparticle solutions changed into transparent from cloudy. After four days, there is no apparent aggregates at the bottom in the three kinds synthetic brine water. By measuring the size of the silica nanoparticles, the silica nanoparticle is stable in the first bottle with NaCl solution. So the right two kinds solution (CaCl₂ solution and synthetic Bakken formation water) were chosen for particle size test. Every sample was tested three times. The results were shown in Table 6.

Table 6. Particle size of silica nanoparticles in CaCl₂ solution and synthetic Bakken formation water

Solution type	Particle Size (nm)		
	First test	Second test	Third test
CaCl ₂ solution	122.7	105.2	117.3
synthetic Bakken formation water	500.3	1255	2625

We can see from the Table 6 that the size of silica nanoparticles in CaCl₂ solution are around its original size 154.1 ± 1.9 nm. This indicates the silica nanoparticle is stable at the experimental condition (salinity: 30,000mg/L CaCl₂ solution, 80°C). The size of silica nanoparticle in synthetic Bakken formation water is much larger than its original size. This indicates the nanoparticle is unstable at the experiment condition (salinity: synthetic Bakken formation water, 80°C). The mainly reason is there are too many ions in the synthetic Bakken formation water, which enhances the chance of collision between ions and silica nanoparticles. After the charge neutralized at the double electric layer of silica nanoparticles, the small nanoparticles can aggregate into big one. This made the size of silica nanoparticles become large.

3.2.4 Lower concentrations of silica nanoparticles (wt%)

Experimental temperature was set at 80°C. The synthetic brine was NaCl solution, and its salinity is 30,000mg/L. In last stability experiment, the silica nanoparticle solution was stable with concentration of 0.05wt%. So we prepared other three different concentrations of silica nanoparticle solutions, i.e. 0.06w%, 0.07wt%, and 0.08wt%. The sample volume was 10ml. This was primarily to test the stability of different concentrations of silica nanoparticles in synthetic brines.

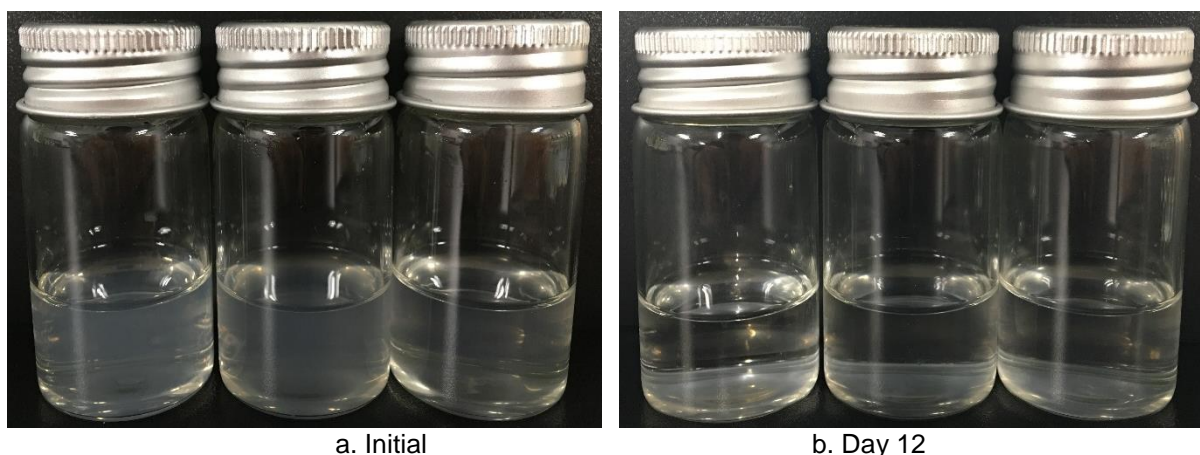


Figure 34. Three different concentrations of silica nanoparticle solutions at initial preparation and Day 12 at 80°C

Initially all three silica nanoparticle solutions were cloudy. The ultrasonic dispersion process was continued for 15 minutes to assure that nanoparticles had been homogenously dispersed. After twelve days, the solution changed, as shown in Figure 34b. The samples from left to right the concentration of silica was 0.06wt%, 0.07wt% and 0.08wt%, respectively.

(1) Particle size measurement with no filtration

After twelve days, there were no apparent sediments at each bottle. Its nanoparticle size and zeta potential were tested to determine whether there was any aggregation in it. The samples were tested four times. The results were shown in Table 7.

Table 7. Particle size and zeta potential of silica nanoparticles solutions of 0.06wt% concentration

Concentration	Particle Size (nm)			
	First test	Second test	Third test	Forth test
0.06%	1181	1086	1057	958.2
	Zeta Potential (mV)			
	First test	Second test	Third test	Forth test
	27.0	24.7	22.6	20.3

We can see from the Table 7 that the size of silica nanoparticles with the concentration of 0.06wt% is much larger than its original size 154.1 ± 1.9 nm. This indicates the silica nanoparticles have aggregated. So the silica nanoparticle is unstable with the concentration higher than 0.06wt% at 80°C. But its zeta potential is positive. Maybe the silica molecule is wrapped by Na^+ . So the zeta potential cannot reflect its real potential situation.

(2) Particle size measurement with filtration

The original zeta potential of silica nanoparticle was about -45.8 ± 3.9 mV. After 12 days at 80°C, zeta potential is positive. Maybe the reason was the silica nanoparticle was wrapped by NaCl crystal. So we filtrated the solution (0.06wt%) with $0.45\mu\text{m}$ cellulose acetate. And the test result is shown in Table 8.

Table 8. Particle size of silica nanoparticle solution of 0.06wt% concentration (after filtration)

Concentration	Particle Size (nm)			
	First test	Second test	Third test	Forth test
0.06%	1218	840.0	622.3	208.9
	Zeta Potential (mV)			
	First test	Second test	Third test	Forth test
	19.0	19.5	21.5	22.7

We can see from the Table 8 that the size of silica nanoparticle with the concentration of 0.06wt% is much larger than its original size 154.1 ± 1.9 nm after filtration with $0.45\mu\text{m}$ cellulose acetate. This indicated the silica nanoparticle had aggregated. And its zeta potential is also positive. Maybe the silica molecule is tightly wrapped by Na^+ . So we should apply other experiment method to test the zeta potential of aggregated silica.

3.2.5 Different cation valence

Experiment temperature was set at 80°C and experimental pressure was 1 atm. The concentration of silica nanoparticles was 0.06wt%. We prepared two kinds of brines, including NaCl solution (30,000mg/L) and CaCl_2 solution (30,000mg/L). The sample volume was 10ml. This was primarily to test the stability of silica nanoparticles in synthetic brines with different cation valences.

Initially all the solutions were transparent. The ultrasonic dispersion process was continued for 15 minutes to assure that nanoparticles had been homogenously dispersed. After twelve days, the solution changed, as shown in Figure 35. The samples from left to right were the NaCl solution and CaCl_2 solution, respectively.

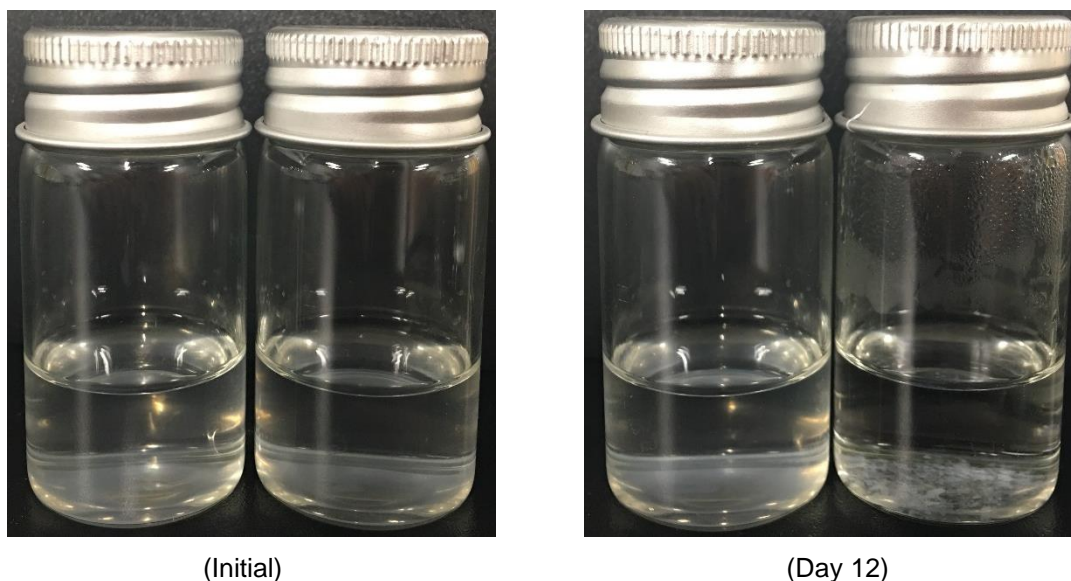


Figure 35. 0.06wt% silica nanoparticle solutions in two kinds of synthetic brines at initial preparation and Day 12 at 80°C

We can see from the Figure 35 that after twelve days, the NaCl solution (that is the first bottle) was still transparent, while the CaCl_2 solution (that is the second bottle) already being some obvious aggregation at the bottle bottom (Figure 36). This indicated divalent cations had greater impact on silica nanoparticle than monovalent cations. This is due to the divalent cations have

strong charge intensity, which neutralizes surface negative charge of silica nanoparticle. When the remaining negative surface charge decreases, the repulsion between molecules of silica nanoparticle reduced, inducing the aggregation.

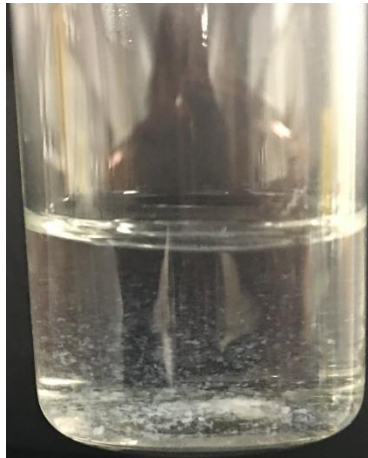


Figure 36. 0.06wt% silica nanoparticle solution in CaCl₂ solution at Day 12 at 80°C

4. Evaluation and optimization of the nanoparticle-surfactant for EOR

4.1 Description of newly purchased nanoparticles

During the last quarter, four new nanoparticles were purchased. Details of nanoparticles are given in Table 9. By doing researches on these four materials, we can study the effects of particle size and type.

Table 9. Nanoparticles

Nanoparticles	Descriptions
ST-O (Silica nanoparticles)	A 20-21 wt.% aqueous dispersion at pH=2-4, spherical, average diameter of approximately 10-20 nm, viscosity<3 mPa.s
ST-30L (Silica nanoparticles)	A 20-21 wt.% aqueous dispersion at pH=9.5-11.0, spherical, average diameter of approximately 40-50 nm, viscosity<3 mPa.s
Aluminasol (Aluminium Oxide)	A 10 wt.% aqueous dispersion at pH=4-6, amorphous, viscosity=50-3000 mPa.s, stabilized by acetic acid (CH ₃ COOH)
TiSol A (Titanium Oxide)	A 14.9 wt.% aqueous dispersion at pH=1.5, amorphous, viscosity=9 mPa.s, average diameter of approximately 54 nm

4.2 Stability test

In this test, API brine composed of 8.0 wt.% NaCl and 2.0 wt.% CaCl₂ were applied to prepare nanofluids with concentrations of 0.02 wt.%, 0.05 wt.%, 0.5 wt.% and 1.0 wt.%, respectively. After mixing, testing samples were put into an ultrasonic dispersion instrument for 10 minutes to ensure uniform dispersion. The experiments were conducted at 80 °C, results were shown in Figure 37.



ST-O, Initial state



ST-O, 24 h at 80 °C



ST-30L, Initial state



ST-30L, 24 h at 80 °C



Aluminasol, Initial state



Aluminasol, 24 h at 80 °C



TiSol A, Initial state



TiSol A, 24 h at 80 °C

Figure 37. Comparative study of stability test

Among the four nanoparticles, silica nanoparticles with smaller size, lower pH and lower concentration was the most stable one. ST-O solutions were stable at initial state with concentration of 0.02 wt.%-1.0 wt.%, and after one-day in the oven, turbidity and some floccules can be witnessed in systems with concentration higher than 0.05 wt.%. It is well known that salts especially bivalent salts can compress the diffused double layer on particle surface, alter the surface charge and promote particle aggregation. Comparing ST-O with ST-30L, solution stability decreased with increasing particle size. Once SL-30L particles were put into API brine, a layer of solid sedimentation can be instantly observed, and the same phenomenon was seen in Aluminasol and TiSol A as well. Due to low stability of particles in brine, many methods have been tried, including the combination of high salt-tolerant surfactants.

4.3 The effects of pH and zeta potential test

Particle concentration was set at 0.4 wt.%. Solution pH were modified by diluted HCl and NaOH to be 1.98, 3.95, 5.65, 6.98, 8.34. Water used in this test was deionized water, whose pH is 5.65 at 20 °C.



ST-O, Initial state



ST-O, 24 h at 80 °C



ST-30L, Initial state



ST-30L, 24 h at 80 °C



TiSol A, Initial state

TiSol A, 24 h at 80 °C

Figure 38. The effect of pH on nanoparticle stability

ST-O has high stability in either acidic or alkaline conditions, after one day's aging at 80 °C, no obvious turbidity or stratification phenomenon. In addition, the characteristics of thermal aged system were verified by particle distribution test and Zeta potential test shown in Figure 39. The optimal pH condition for ST-O is around 5.65. Simply seen from bottle test, the five ST-30L samples also exhibited relatively high transmittance, and there is no sharp increase in particle diameter and Zeta potential as well, results of the three tests have good coherence to each other. As for Tisol A solution, higher stability was shown in acidic conditions, and its size nearly doubled when pH increase from 6.98 to 8.34, accompanied by noticeable turbidity.

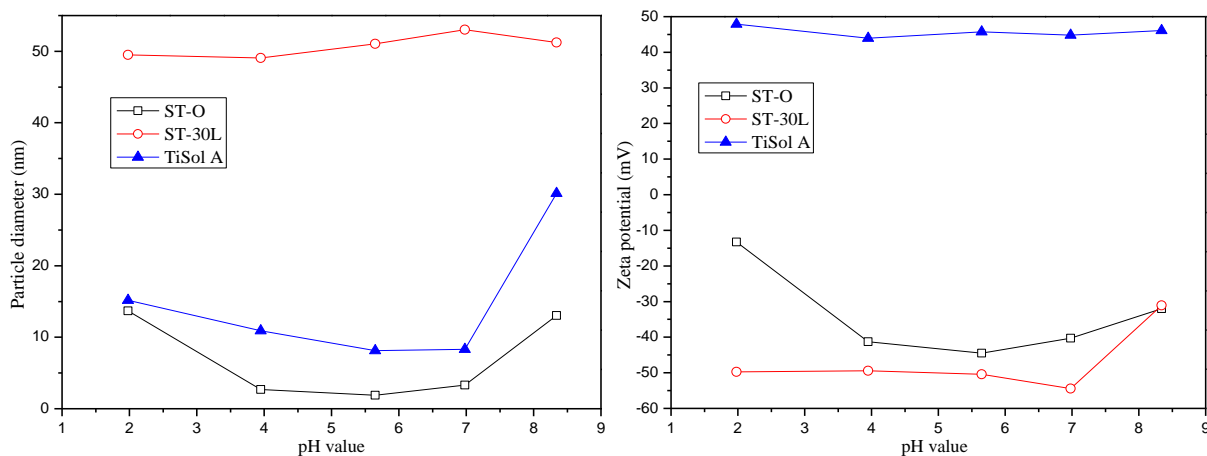


Figure 39. Diameter and Zeta potential of thermal aged systems

4.4 Emulsion test

CTAB, short for Cetyltrimethyl Ammonium Bromide, is a normally used cationic surfactant and its critical micelle concentration is 0.9 mM (0.0335 wt.%) in water at 30 °C. Because silica nanoparticle is negatively charged, so CTAB can surely absorb on the surface of silica nanoparticles through electrostatic interaction. Due to the decrease of zeta potential and repulsive force between particles, small particles aggregation is inevitable, as elaborated in Figure 40, the formula of samples is 10 mL solutions of DI, 1%SiO₂, 0.1%CTAB, 1%SiO₂+0.018%CTAB, 1%SiO₂+0.0335%CTAB, 1% SiO₂+0.0546%CTAB from left to right.



Initial state

24 h at 80 °C

Figure 40. Mixtures of silica dioxide and CTAB

The thickness of sedimentation layer decreased with increasing CTAB concentration, mainly because of the increasing reduction in zeta potential and larger particles are easier to form in such situations. Though particle dispersing performance became worse with the addition of opposite charged chemicals, its capacity to stabilize emulsions increased.

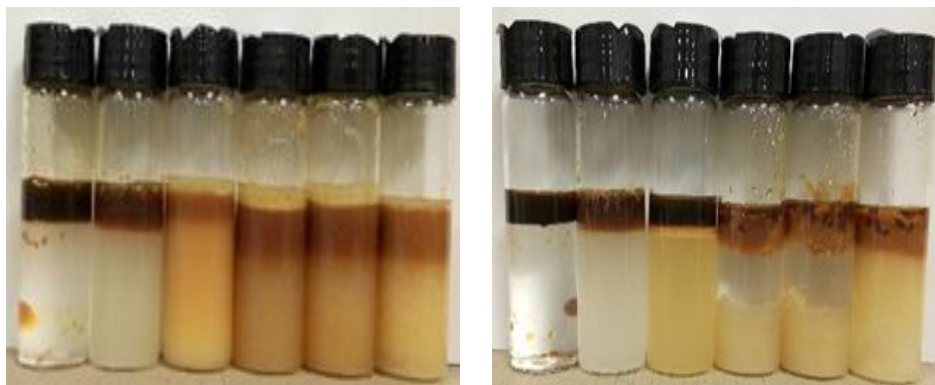


Figure 41. Emulsion test of silica dioxide and CTAB mixtures

As shown in Figure 41, deionized water and strong hydrophilic particles (pure 1.0 wt.% silica dioxide) cannot stabilize emulsions. After settling on the table for a few hours at room temperature, the mixture quickly became two separated phases. CTAB alone can dissolve a small amount of oil into water. Interestingly, with the introduction of nanoparticles, larger volume of emulsion can be obtained with less surfactant. However, the emulsion size is much larger than that stabilized by surfactant alone, which is more likely to induce negative Jamin effect especially in tight reservoirs. So, when adopting nanoparticle-surfactant system for shale oil exploitation, less emulsions might induce the better results. Some pictures of emulsion morphology were presented in Figure 42.

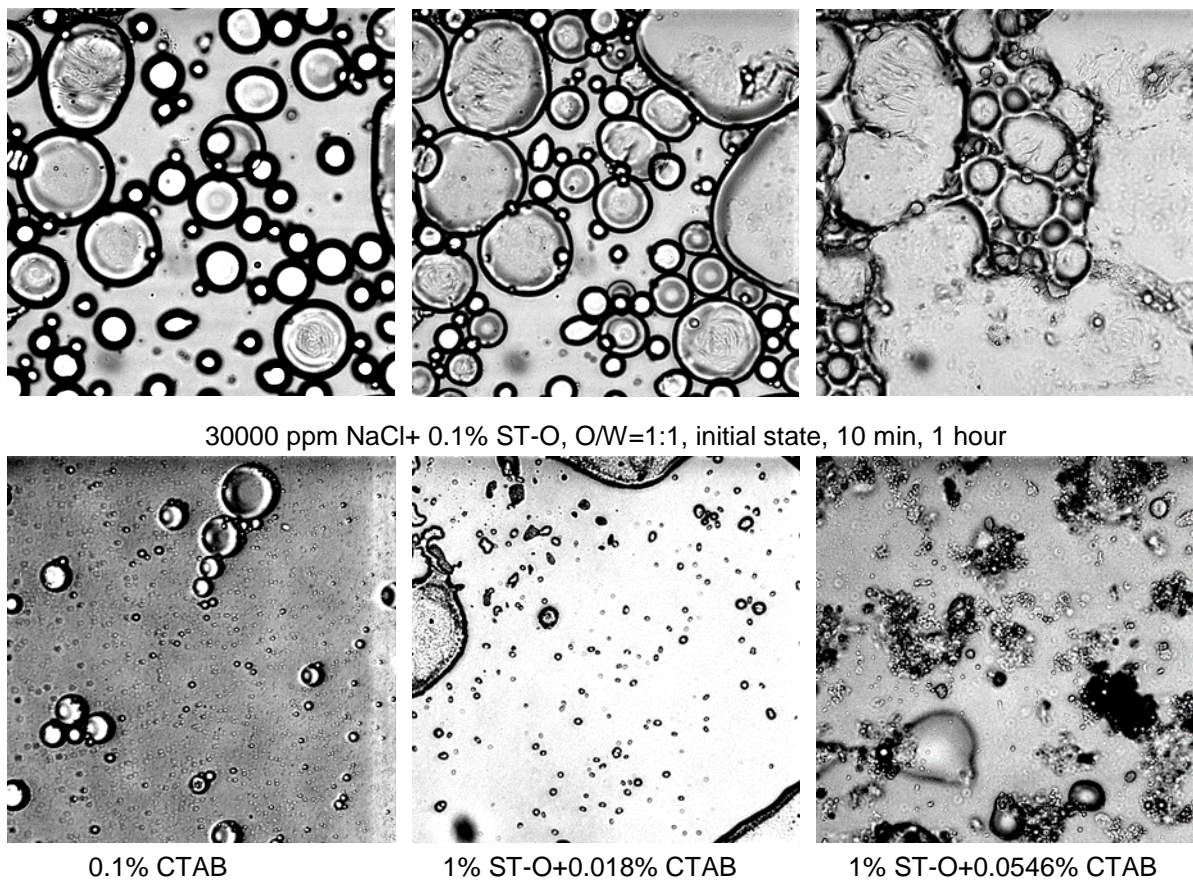


Figure 42. Emulsion morphology under microscope

5. Preparation and characterization of small silica nanoparticles for oil recovery

5.1 Introduction

The size of silica nanoparticles that was tested in our last report was too large to penetrate into the pores of the rock. Therefore, we were trying to develop silica nanoparticles as small as possible in this quarter.

5.2 Experimental section

Materials. Tetraethylorthosilicate, cyclohexane, NH_4Cl , and NH_4OH were purchased from Sigma Aldrich.

Instrumentations. An Eppendorf 5804 centrifuge and ultrasonicator were used to wash the silica nanoparticles. A Zetasizer particle analyzer (Marlwen, Nano-ZS) was used to characterize the hydrodynamic diameter and zeta potential of nanoparticles. A SEM was utilized to obtain the morphology of the silica nanoparticles.

Synthesis of the small silica nanoparticles. Certain amount of ammonia was added into 40 mL of 8 mM NH_4Cl solution until the final pH value was adjusted to 9.8. The solution was transferred into a 40 °C water bath and stirred for 30 min. Then, 6 mL of TEOS and 3 mL of cyclohexane were added into the above solution under vigorous stirring. After the reaction time for 24 hours, the nanoparticles were washed by ethanol and water for 3 times.

5.3 Results and discussion

As we discussed in the section 2 of this report, we found that the pore size of the rock ranges from several nanometers to 40 nanometers, which meant that the previous nanoparticles we prepared were too large for the project. Therefore, we utilized new method for the preparation of small silica nanoparticles. As shown in Figure 43, the hydrodynamic diameter was found to be around 28 nm, which is much smaller than that synthesized by the Stober method in our previous reports. Meanwhile, the zeta potential of the silica nanoparticles was about -53 mV, which is similar to the previous silica nanoparticles (Figure 44).

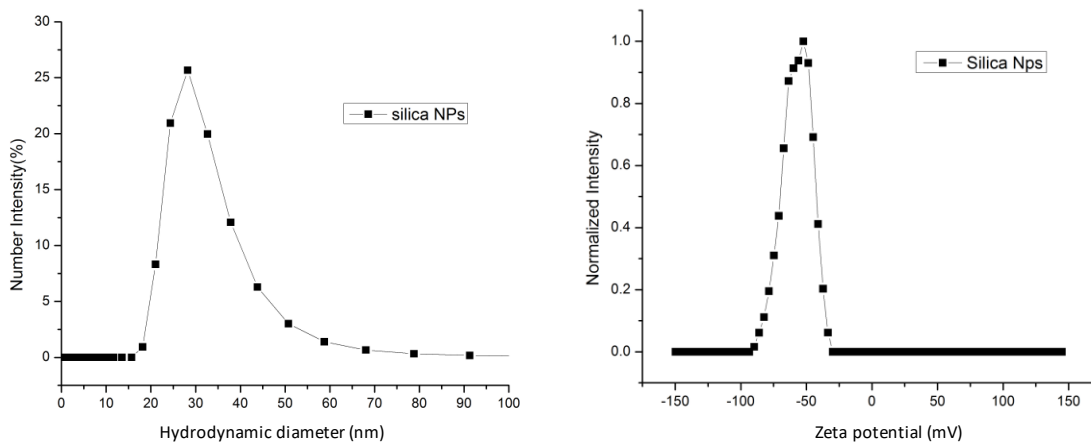


Figure 43. Hydrodynamic diameter of silica nanoparticles **Figure 44.** Zeta potential of silica nanoparticles

We also used SEM to observe the morphology and the size of the prepared silica nanoparticles. As shown in Figure 45, the size from SEM images were consistent with that for DLS measurement, ensuring the small size of the proposed silica nanoparticles.

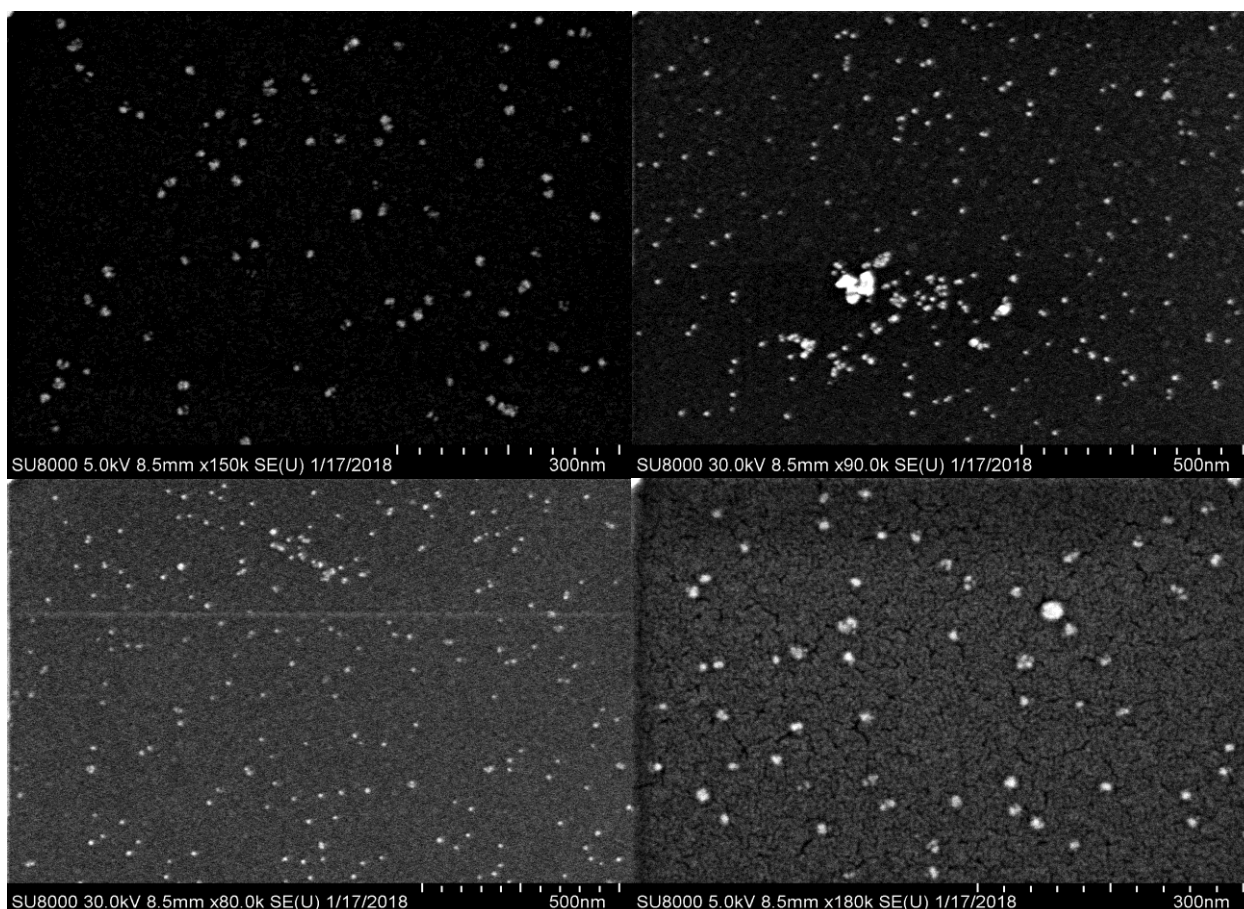


Figure 45. The SEM images of the silica with different magnification.

6. Preparation and characterization of small polymer nanoparticles for oil recovery

6.1 Introduction

Polymer nanoparticles are another important type of nanomaterials that might have the potential for oil recovery. First of all, the size of the polymer nanoparticles can be decreased to as small as close to 10 nm. Second, the polymer nanoparticles can be easily modified with surfactant by the hydrophobic interactions, which might have the similar binding force with the oil.

6.2 Experimental section

Materials. poly(9-vinylcarbazole) (PVK), Poly(styrene-co-maleic anhydride), cumene terminated (PSMA) were purchased from Sigma Aldrich.

Instrumentations. A Zetasizer particle analyzer (Marlwen, Nano-ZS) was used to characterize the hydrodynamic diameter and zeta potential of nanoparticles.

Synthesis of the small polymer nanoparticles. 5 mL THF solution containing 100 ppm PVK, 20 ppm PSMA were mixed thoroughly. Then, the THF was injected into 10 mL water under ultrasonic for 1 min. The TFH was removed by blowing with nitrogen for 2 hours.

6.3 Results and discussion

At this stage, we just started the preparation of the polymer nanoparticles. Only the hydrodynamic size was investigated. As shown in Figure 46, the size of polymer nanoparticles was about 25 nm, which has the potential to penetrate into the pores of the rocks.

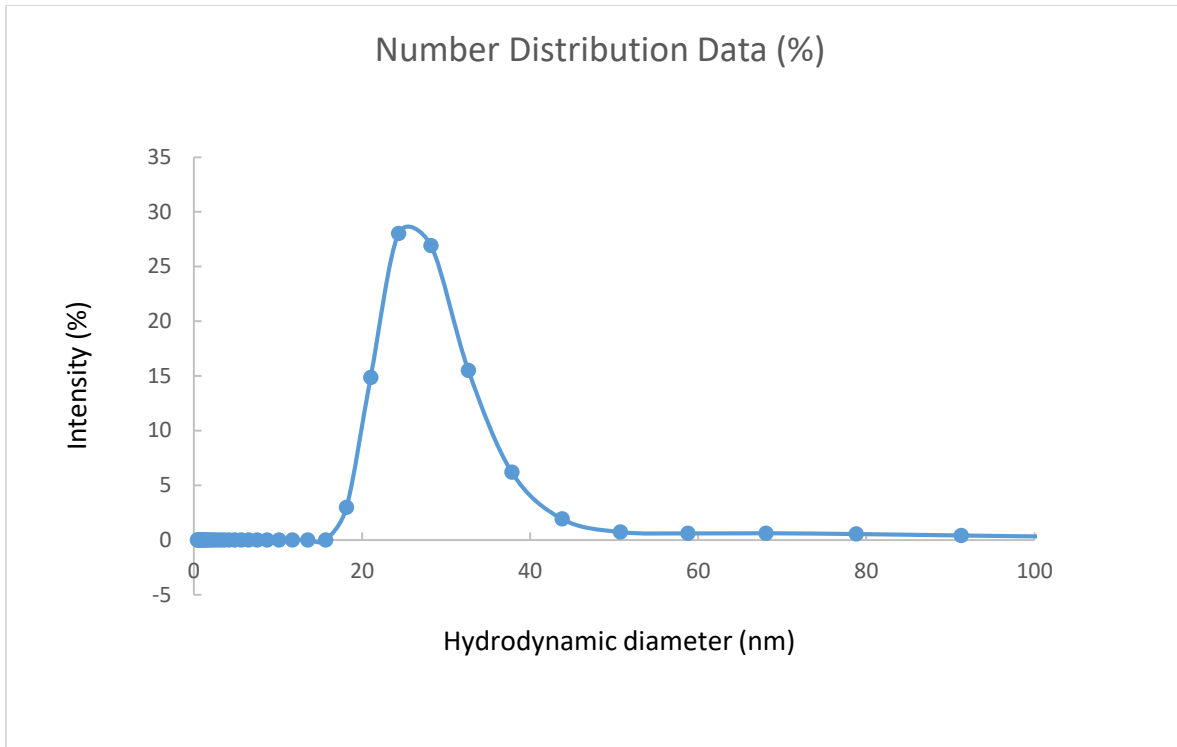


Figure 46. The hydrodynamic diameter of the polymer nanoparticles.

We will keep on working the polymer nanoparticles in the next quarter to investigate its stability and potential to carry oil from the rocks.

Future Work

1. Nanoscale simulation of fluid properties in tight formations.
2. Interfacial tension between oil and water made up of different nanoparticles.
3. The synergistic effect of surfactant and nanoparticles.
4. Recovery by different kinds of surfactant and nanoparticles.
5. Adsorption of different kinds of surfactant and nanoparticles.
6. How to modify the properties of nanoparticles and surfactants to make them applicable in high salinity brine.

References

- Adam De Gree. 2015. The History and Working Principle of the Scanning Electron Microscope (SEM). Presented at the AZONANO, 3-20 Mar.
- Andreani, T.; Souza, A. L. R. d.; Kiill, C. P.; Lorenzón, E. N.; Fanguero, J. F.; Calpena, A. C.; Chaud, M. V.; Garcia, M. L.; Gremião, M. P. D.; Silva, A. M.; Souto, E. B., Preparation and characterization of PEG-coated silica nanoparticles for oral insulin delivery. *International Journal of Pharmaceutics* 2014, 473 (1), 627-635.
- Aoudia M., Al-Maamari R. S., Nabipour M., Al-Bemani A. S.. Laboratory study of alkyl ether sulfonates for improved oil recovery in high-salinity carbonate reservoirs: A case study. *Energy Fuels* 2010, 24, 3655-3660.
- Aveyard R, Clint JH, Nees D, Paunov VN. Compression and structure of monolayers of charged latex particles at air-water and octane-water interfaces. *Langmuir* 2000, 16, 1969-1979.
- Binks BP, Lumsdon SO. Effects of oil type and aqueous phase composition on oil-water mixtures containing particles of intermediate hydrophobicity. *Phys Chem* 2000, 2, 2959-2967.
- Binks BP, Lumsdon SO. Influence of particle wettability on the type and stability of surfactant-free emulsions. *Langmuir* 2000, 16, 8622-8631.
- Brown ABD, Smith CG, Rennie AR. Fabricating colloidal particles with photolithography and their interactions at an Air-water interface. *Phys Rev E* 2000, 62, 951-960.
- Brunauer S, Emmett PH, Teller E. Adsorption of gases in layers. *Journal of the American Chemical Society*. 1938, 60(2), 309-319.
- Chen, X., Cao, G., Han, A. et al. 2008. Nanoscale Fluid Transport: Size and Rate Effects. *Nano Letter* 8(9):2988-2992.
- Firincioglu, T., Ozkan, E., and Ozgen, C. 2012. Thermodynamics of Multiphase Flow in Unconventional Liquid-Rich Reservoirs. Presented at the SPE Annual Technical Conference and Exhibition, San Antonio, Texas, 8-10 October. SPE-159869-MS.
- Gallagher PD, Maher JV. Partitioning of polystyrene latex spheres in immiscible critical liquid mixtures. *Phys Rev A* 1992, 46, 2012-2021.
- Goldstein, G. I.; Newbury, D. E.; Echlin, P.; Joy, D. C.; Fiori, C.; Lifshin, E. *Scanning electron microscopy and x-ray microanalysis*; Plenum Press: New York, 1981.
- Haiping Lu, Chris Haugen, and Tim Garza, Jeffrey Russek, Chad Harbaugh, SPE169805 Test Method Development and Scale Inhibitor Evaluations for High-Salinity Brines in the Williston Basin, SPE International Oilfield Scale Conference and Exhibition held in Aberdeen, Scotland, UK, 14-15 May 2014
- Hamada, Y., Koga, K., and Tanaka, H. 2007. Phase Equilibria and Interfacial Tension of Fluids Confined in Narrow Pores. *H. Chemical Physics* 127: 084908.
- Hewakuruppu, Y. L., Dombrovsky, L. A., Chen, C., Timchenko, V., Jiang, X., Baek, S., Taylor, R. A.. Plasmonic pump-probe method to study semi-transparent nanofluids. *Applied Optics*. 2013, 52 (24): 6041-6050.
- J.H.M. Bonnie and T.W. Fens, Koninklijke/Shell Exploratie en Productie Laboratorium. 1992. Porosity and Permeability from SEM Based Image Analysis of Core Material. SPE 23619.
- Kanda, H., Miyahara, M., and Higashitani, K. 2004. Triple Point of Lennard-Jones Fluid in Split Nanopore: Solidification of Critical Condensate. *J. Chem. Phys.* 120(13): 6173-6179.
- Karen M. Steel, Robin E. Dawson, David R. Jenkins, Robin Pearce and Merrick R. Mahoney. 2017. Use of rheometry and micro-CT analysis to understand pore structure development in coke. Presented at the Fuel Processing Technology: 106-113.
- Karimi A., Fakhroueian Z., Bahramian A., et al. Wettability alteration in carbonates using zirconium oxide nanofluids: EOR implications. *Energy Fuels* 2012, 26, 1028-1036.

Li, S.; Hendraningrat, L.; Torsaeter, O., Improved Oil Recovery by Hydrophilic Silica Nanoparticles Suspension: 2-Phase Flow Experimental Studies. International Petroleum Technology Conference, 2013.

Liu Jianjun, Lin Lijun, Ji Youjun. 2011. Using Rock SEM Image to Create Pore-scale Finite Element Calculation Mesh. International Conference on Physics Science and Technology

Mohammad Z., Riyaz K., Nasim B.. Enhancement of surfactant flooding performance by the use of silica nanoparticles. *Fuel*, 2015, 143: 21-27.

Moore, E. B., de La Llave, E., Welke, K. et al. 2010. Freezing, Melting and Structure of Ice in a Hydrophilic Nanopore. *Physical Chemistry Chemical Physics* 12 (16): 4124-4134.

Nurudeen Y., Muhammad A. M., Ahmad K. I.. Experimental investigation of minimization in surfactant adsorption and improvement in surfactant-foam stability in presence of silicon dioxide and aluminum oxide nanoparticles. *Journal of Petroleum Science and Engineering*, 2017, 159: 115-134.

Qiao, Y., Punyamurtula, V K., Han, A. et al. 2006. Temperature Dependence of Working Pressure of a Nanoporous Liquid Spring. *Applied Physics Letters* 89 (25):251905-251905.

Reimer, L. Scanning electron microscopy: physics of image formation and microanalysis; Springer, 1998.

Schramm L. L. Surfactants: fundamentals and applications in the petroleum industry. United Kingdom; 2000.

Schwartz H, Harel Y, Efrima S. Surface behavior and buckling of silver interfacial colloid films. *Langmuir* 2001,17,3884-3892.

Shahrabadi A., Bagherzadeh H., Roustaei A., Golghanddashti H.. Experimental investigation of HLP nanofluid potential to enhance oil recovery: A mechanistic approach. Society for Petroleum Engineers (SPE) Conference Paper SPE-156642-MS, 2012, DOI: <http://dx.doi.org/10.2118/156642-MS>.

Sing, K.S.W. Reporting physisorption data for gas/solid systems with special reference to the determination of surface area and porosity. *Pure Appl. Chem.* 1985, 57(4), 603–619.

Suleimanov B. A., Ismailov F. S., Veliyev E. F.. Nanofluid for enhanced oil recovery. *Journal of Petroleum Science and Engineering* 2011, 78: 431-437.

Theloy, C., Sonnenberg, S.A., SPE 168870 Integrating Geology and Engineering: Implications for Production in the Bakken Play, Williston Basin, Unconventional Resources Technology Conference, Denver, Colorado 12-14 August 2013.

Utah State University Microscopy Core Facility.

Wasan D. T., Nikolov A. D.. Spreading of nanofluids on solids. *Nature* 2003, 423, 156-159.

W.D Clelland and T.W Fens, Koninklijke/Shell E&P Laboratorium. 1991. Automated Rock Characterization With SEM/Image-Analysis Techniques.

Wong K. V., Leon O. Applications of nanofluids: Current and future. *Advanced Mechanical Engineering*, 2010, 1-11.

Yaniv, K., Uri, N. 2014. Quantification of poresize distribution using diffusion NMR: Experimental design and physical insights. *The Journal of Chemical Physics* 140, 164201.

Yu H., Kotsmar C., Yoon K. Y., et al. Transport and retention of aqueous dispersions of paramagnetic nanoparticles in reservoir rocks. In: SPE improved oil recovery symposium, Tulsa, OK, USA; 2010.

Zarragoicoechea, G. J. and Kuz, V. A. 2004. Critical Shift of Confined Fluid in a Nanopore. *Fluid Phase Equilibria* 220: 7-9.